

Manuscript Number: JALCOM-D-19-07405R1

Title: Microstructure evolution and enhanced creep property of a high Nb containing TiAl alloy with carbon addition

Article Type: Full Length Article

Keywords: TiAl alloys; precipitation; phase transitions; creep properties; transmission electron microscopy, TEM; synchrotron radiation

Corresponding Author: Professor Lin Song, Ph.D.

Corresponding Author's Institution: Northwestern Polytechnical University

First Author: Lin Song, Ph.D.

Order of Authors: Lin Song, Ph.D.; Xinguo Hu; Li Wang; Andreas Stark; Daria Lazurenko; Uwe Lorenz; Junpin Lin; Florian Pyczak; Tiebang Zhang

Abstract: The microstructure evolution and carbide precipitation in a Ti-46Al-8Nb-0.7C alloy as well as its creep properties at intermediate temperatures are investigated by high-energy X-ray diffraction and electron microscopy. The alloy with a nearly fully lamellar microstructure exhibits excellent creep resistance, which could be attributed to the good microstructural stability and strengthening effects from both P- and H-carbides. It is also found that the creep parameters have different effects on the precipitation of the carbides. The overall volume fraction of the carbides shows a positive correlation with the creep temperature and time. However, the thermal stability of P-carbides in the γ grain interior decreases at a higher creep temperature. The creep stress hardly affects the precipitation and morphology development of the P-carbides. On the contrary, a higher stress can promote the H-carbide formation at the γ/α_2 interfaces via α_2 lath decomposition in lamellar colonies.

Research Data Related to this Submission

There are no linked research data sets for this submission. The following reason is given:

Data will be made available on request

To: Editor of Journal of Alloys and Compounds

From: Lin Song

State Key Laboratory of Solidification Processing,

Northwestern Polytechnical University,

No. 127 Youyixi Road, Xi'an, Shaanxi 710072, China

Response to the comments on JALCOM-D-19-07405

“Microstructure evolution and enhanced creep property of a high Nb containing TiAl alloy with carbon addition”

Dear editor:

We have received reviewers' comments on our manuscript. We would like to take this opportunity to thank you and the reviewers for refereeing our manuscript. According to their comments, we have revised the paper and the main responses are as follows.

(All the lines and pages refer to the revised manuscript)

Response to Reviewer 1's comments:

This paper is systematically investigated the effect of carbide precipitates on creep properties of Ti-46Al-8Nb-0.7C alloy in the temperature range of 750 - 850oC using XRD, SEM as well as TEM. The analysis used in this paper is quite well organized and carefully done, and it turned out to very meaningful discussion. This paper is quite well matched with the qualification of JALCOM and it should be recommended for publication with some minor corrections.

We thank the reviewer for the constructive suggestions and thoughtful comments. In the following, we respond to the comments point-by-point. We also indicate the changes in the revised manuscript.

1. In the keywords, 'TiAl' and 'creep properties' should be included.

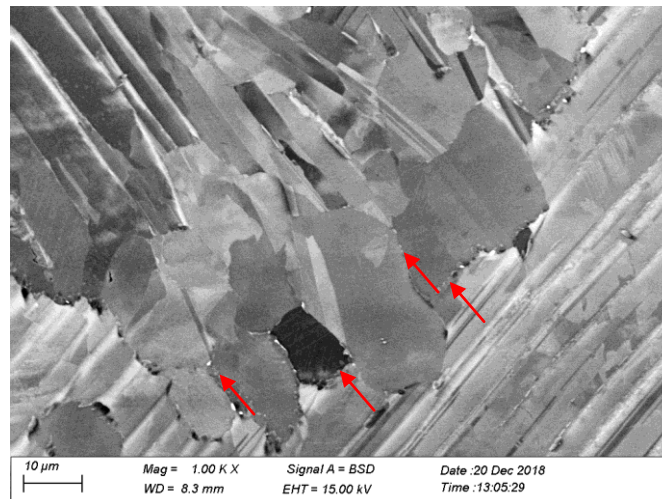
Reply: We have replaced “intermetallics” with “TiAl alloys” and added “creep properties” in the Keywords.

2. In Fig. 1a, what do the red arrows indicate? Are they pointing H-carbides? If so, it would be better including the figure caption.

Reply: We have included the indication of the red arrows in Fig. 1 in the figure caption: “Microstructure and phase constitution of the as-HIPed sample. (a, b) SEM images in back-scattered electron mode (the arrows in (a) and (b) indicate the locations of the H-carbides and the fractured α_2 laths, respectively); (c) HEXRD spectrum, the {106} peak of H-carbides is observed.”

3. In section 3.3.1, the authors mentioned coarsened P-carbides formed at G. B. What are the P-carbides in Fig. 4? Can authors indicate them in the SEM figure?

Reply: Coarsen P-carbides at grain boundaries can be observed by SEM investigation, as indicated in the following image in the specimen after creep at 850 °C and 130 MPa for 3267 h.



In Figure 4, although the majority of the images show the fully lamellar structure, we have indicated the existence of the P-carbides at grain boundaries in Fig. 4f. Since there are a couple of images showing the carbides, we do not specifically note this in the caption, but mention it in the text: **Page6 Line1:** “Due to the large sizes, some coarsened P-carbides at grain boundaries can also be identified in the SEM images (for example at grain boundaries in Fig. 4f).”

4. In section 3.3.2, the authors calculated the weight fraction of composed phases. Is the weight percent is true not volume fraction? Then, how did the authors calculate weight fraction?

Reply: Yes, the result we get is the weight fraction. We calculated the weight fraction of the phase constitutions by Rietveld analysis. And the weight fraction was a direct read out from the analysis results. We think the statement of weight fraction can be remained since the volume fraction and weight fraction are just different ways to show the results.

This is indicated in the experiments part in **Page4 Line5**: “The beam size was 0.5 mm × 0.5 mm and the wavelength 0.14235 Å. The reflections were recorded with a PerkinElmer XRD 1621 flat panel detector. **The weight fractions of the majority phases (γ and α_2) was analyzed by the Rietveld method, while the fractions of the P- and H-carbides could not be determined using this method due to their small contents.**”

5. The creep properties of Ti-46Al-8Nb-0.7C alloy shown in 750, 850oC are good enough for aerospace and automobile application of the alloy? What is the target temperature of the alloy? Also, have other properties such as LCF and HCF reported before?

Reply: Indeed, the creep properties of this alloy seem very promising. As we mentioned in the manuscript, the high amount of C and large-sized lamellar colonies are the reasons for that. However, due to this issue, we expect this alloy may be of low room-temperature ductility and fracture toughness, although we have not measured them yet. The fatigue properties are not tested either. Therefore, we expect if some components do not have strict requirements on the ductility and toughness, this alloy could be used in the range of 750-850°C with stress less than 260MPa. Anyway, a lot of work needs to be done.

Response to Reviewer 2's comments:

TiAl alloys are considered to be promising candidates for current used Ni-based alloys in aerospace and automobile industries because of their outstanding advantages, such as low density, high strength, excellent oxidation resistance. The finally realized applications of

current engineering gammalloy materials (cast 4822, cast 45XD and wrought TNM) as aero-engine low pressure turbine blades for intermediate service temperatures (up to 750°C) began to establish the foundations of their respective materials-processes- manufacturing technologies. Nb addition could improve high temperature properties in high-Nb TiAl alloys. However, the lack of structure stability at elevated temperatures limit their wider applications. The present paper focuses on the microstructure evolution and carbide precipitation in a Ti-46Al-8Nb-0.7C alloy as well as its creep properties at intermediate temperatures. The results show that the alloy with a nearly fully lamellar microstructure exhibits excellent creep resistance, which could be attributed to the good microstructural stability and strengthening effects from both P- and H-carbides. This work is interesting and possible to help the designing the new class of the alloys for higher service temperature Therefor it is worth to be accepted for publication in the Journal of Alloys and Compounds.

Reply: We sincerely appreciate the positive comments from the reviewer.

If there is any question please do not hesitate to contact us as soon as possible. We all the co-authors are looking forward to hearing from you.

Thank you!

Yours sincerely

Lin Song on behalf of all the authors.

1 **Microstructure evolution and enhanced creep property of a high Nb containing**
2 **TiAl alloy with carbon addition**

3
4 Lin Song^{1,2*}, Xinguo Hu¹, Li Wang^{2*}, Andreas Stark², Daria Lazurenko³, Uwe
5 Lorenz², Junpin Lin⁴, Florian Pyczak², Tiebang Zhang¹

6
7 ¹State Key Laboratory of Solidification Processing, Northwestern Polytechnical
8 University, Xi'an, Shaanxi 710072, China

9 ²Institute of Materials Research, Helmholtz-Zentrum Geesthacht, Max Planck-Str. 1,
10 Geesthacht, D-21502, Germany

11 ³Novosibirsk State Technical University, Karl Marks str. 20, Novosibirsk, 630073,
12 Russia

13 ⁴State Key Laboratory for Advanced Metals and Materials, University of Science and
14 Technology Beijing, Beijing 100083, China

15 Corresponding authors: Lin Song (songlin@nwpu.edu.cn, lin.song@hzg.de), Li Wang
16 (li.wang1@hzg.de)

17
18 **Abstract**

19 The microstructure evolution and carbide precipitation in a Ti-46Al-8Nb-0.7C alloy
20 as well as its creep properties at intermediate temperatures are investigated by
21 high-energy X-ray diffraction and electron microscopy. The alloy with a nearly fully
22 lamellar microstructure exhibits excellent creep resistance, which could be attributed
23 to the good microstructural stability and strengthening effects from both P- and
24 H-carbides. It is also found that the creep parameters have different effects on the
25 precipitation of the carbides. The overall volume fraction of the carbides shows a
26 positive correlation with the creep temperature and time. However, the thermal
27 stability of P-carbides in the γ grain interior decreases at a higher creep temperature.
28 The creep stress hardly affects the precipitation and morphology development of the
29 P-carbides. On the contrary, a higher stress can promote the H-carbide formation at
30 the γ/α_2 interfaces via α_2 lath decomposition in lamellar colonies.

31
32 **Keywords**

33 **TiAl alloys**; precipitation; phase transitions; **creep properties**; transmission electron
34 microscopy, TEM; synchrotron radiation.

35
36 **1. Introduction**

37 As a new class of intermetallic structural materials, high Nb-containing TiAl alloys
38 (high Nb-TiAl alloys) have achieved significant development in the recent years and

1 show promising applications in the aerospace and automotive markets [1-4].
2 Systematical studies have been conducted to understand and improve the creep
3 behavior of high Nb-TiAl alloys [5-9]. Numerous studies revealed that the fully
4 lamellar microstructure with high amounts of anisotropic laths showed better creep
5 resistance than the nearly lamellar and duplex microstructures [4, 10]. Meanwhile, the
6 microstructural stability is important for the creep life of high Nb-TiAl alloys. For
7 blade application, γ -TiAl alloys are expected to have a good microstructure stability to
8 achieve a long creep life with a small creep strain [3]. The microstructural degradation
9 via the decomposition of α_2 laths and the discontinuous precipitation at lamellar
10 boundaries during the creep process deteriorates the creep resistance significantly
11 [10-12]. Thus, a better creep strength can be achieved by appropriate alloying and
12 annealing treatment to stabilize the microstructure. Zhu et al. reported that after
13 annealing a Ti-47Al-2Nb-2Mn (all compositions are given in at.% unless indicated
14 otherwise) + 0.8 vol.% TiB₂ alloy at 1000 °C for 8 h the microstructure was
15 destabilized due to the volume fraction decrease of the α_2 phase, resulting in a better
16 creep resistance than the microstructure without annealing treatment [10]. The creep
17 resistance of a Ti-43.5Al-4Nb-1Mo-0.1B-0.3C-0.3Si alloy was enhanced by
18 decreasing the lamellar interface spacing as the lamellae interfaces impeded the
19 motion of ordinary dislocations [8]. However, Zhu et al. reported that the lamellar
20 refinement was important for improving the creep resistance at primary creep stage in
21 a Ti-45Al-2Nb-2Mn+0.8 vol.% TiB₂ alloy, but detrimental for the total creep life since
22 the fine lamellar microstructure was susceptible to deformation-induced
23 spheroidization [13]. Besides, the equiaxed grains at lamellar boundaries which were
24 resulted from spheroidization provoked easy dislocation motion and deteriorated the
25 creep resistance [11]. Thus, the further enhancement of creep resistance can be
26 obtained by microstructural optimization. It is reported that carbon addition can
27 improve the creep properties of TiAl alloys via solid-solution and precipitation
28 strengthening depending on the carbon content [14-17]. Klein et al. claimed that the
29 addition of carbon stabilized the α_2 phase and hindered the precipitation of γ and β_0
30 (ω_0) phases [18]. Park et al. reported that the addition of carbon increased the
31 heterogeneous nucleation rate of the γ laths effectively, resulting in a reduction of the
32 lamellar spacing within the lamellar colonies and thus improving the creep resistance
33 [19]. During the annealing and creep processes, the perovskite (P-) type carbides and
34 hexagonal (H-) type carbides precipitate in the γ phase, at the lamellar interfaces and
35 grain boundaries. It is believed that the carbides are effective pinning obstacles for
36 dislocations in carbon containing TiAl alloys [15, 17, 20]. Schwaighofer et al. found
37 that some P-carbides nucleated at dislocations, which were deformation-induced
38 during creep [15]. Christoph et al. revealed that a fine dispersions of P-carbides
39 formed arrays of strong glide obstacles for perfect and twinning partial dislocations

1 after compression at room temperature [17]. Wang et al. reported that the P-carbides
2 undergone continuous morphology development when annealed at a temperature
3 range from 800 to 1000 °C [21-23]. It is found that the P-carbides grew, coarsened
4 and split eventually during annealing [22, 23]. H-carbides usually form at grain
5 boundaries and in the γ grains with coarse particle size with the relationship
6 $[101]\gamma//[11\bar{2}0]H$; $(11\bar{1})\gamma//(0001)H$ [23]. Lapin et al. claimed that the formation of
7 primary H-carbides could improve the creep resistance of Ti-46.4Al-5.1Nb-1C-0.2B
8 alloy during creep from 800 to 950 °C [24]. However, the morphology development
9 of carbides during creep still needs further investigation. Besides, the effects of creep
10 parameters on the formation of P-carbides and H-carbides are still not clear.

11 In the present work, the strengthening mechanisms and microstructure evolution in
12 the C-containing high Nb-TiAl alloys during creep are characterized. The effects of
13 the creep temperature and stress on the stability of the lamellar structure and
14 formation of P- and H-carbides are also discussed. The results of this study could be
15 instructive for further improving the creep properties of TiAl alloys with addition of
16 carbon.

18 **2. Experimental details**

19 The alloy with a nominal composition of Ti-46Al-8Nb-0.7C was prepared in a
20 non-consumable arc melting furnace in an argon atmosphere. A cylindrical ingot
21 measured about $\Phi 130$ mm \times 300 mm was re-melted 4 times to ensure compositional
22 homogeneity. Then the ingot was hot isostatic pressing (HIPed) at 1270 °C under a
23 pressure of 130 MPa for 4 h and then cooled in furnace. Cylinder samples with a size
24 of 10 mm in diameter and a gauge section of $\Phi 5.3\times 27.3$ mm were cut for creep tests
25 from the center of the upper part of the as-HIPed ingot. The creep tests were
26 performed under a constant load in a SATEC M3 creep machine at 750 and 850 °C
27 under tensile loading of 130 and 260 MPa in air. To study the microstructural
28 evolution during creep, four creep tests were interrupted before specimen failure. Two
29 tests were stopped at a creep time of 1200 h at 750 °C under 130 and 260 MPa and the
30 other two were interrupted at a creep time of 110 h under 850 °C/260 MPa and 1100 h
31 under 850 °C/130 MPa. All the specimens after the creep test were cut into two parts,
32 namely the gauge and holder section. The gauge section was the loaded part with
33 stress and thermal exposure applied while the holder section was the specimen head
34 used to mount it in the creep machine, which only underwent thermal exposure at the
35 creep temperature. The microstructures before and after the creep tests were
36 investigated on a Zeiss GEMINI 1530 field emission scanning electron microscope
37 (SEM) using the back-scattered electron (BSE) mode and on a FEI Titan 80-300 field
38 emission transmission electron microscope (TEM) operated at 300 kV. The SEM and
39 TEM samples were cut along and perpendicular to the loading direction, respectively.

1 Thin TEM foils were mechanically ground to 0.1 mm and then prepared by twin-jet
2 electro-polishing in a solution of 30 ml perchloric acid, 175 ml butanol, and 300 ml
3 methanol at 30 V and -30 °C. Room-temperature high-energy X-ray diffraction
4 (HEXRD) measurements were conducted at the HEMS beam line run by the
5 Helmholtz-Zentrum Geesthacht at the Deutsches Elektronen-Synchrotron (DESY) in
6 Hamburg. The beam size was 0.5 mm × 0.5 mm and the wavelength 0.14235 Å. The
7 reflections were recorded with a PerkinElmer XRD 1621 flat panel detector. **The**
8 **weight fractions of the majority phases (γ and α_2) was analyzed by the Rietveld**
9 **method, while the fractions of the P- and H-carbides could not be determined using**
10 **this method due to their small contents.**

12 3. Results and discussion

14 3.1 As-HIPed microstructure

15 Fig. 1 shows the microstructure and phase constitution of the as-HIPed sample before
16 creep test. A nearly fully lamellar microstructure composed of large lamellar colonies
17 and a small amount of equiaxed γ grains is shown in Fig. 1a. The average size of the
18 lamellar colonies is about 200 μm . The β_0 and ω_0 phases, which are frequently found
19 in high Nb-containing TiAl alloys, are not observed [25, 26]. As marked by the arrows
20 in Fig. 1b, some fractured α_2 laths are observed at the lamellar colonies, which formed
21 during the furnace cooling process after HIP via the “parallel decomposition”
22 mechanism [27, 28]. In addition, some needle- or plate-like dark features marked in
23 Fig. 1a can be observed, which might be due to the falling out of the large H-carbides
24 during specimen preparation. According to the HEXRD spectrum shown in Fig. 1c,
25 the diffraction peak of {106} planes of the H-carbides is clearly detected, while no
26 reflections from the P-carbides show up. On the contrary, in our previous studies in
27 the HIPed Ti-45Al-5Nb-0.75C alloy with a similar carbon concentration, H-carbides
28 were only occasionally observed while P-carbides were commonly detected at grain
29 boundaries [29, 30]. By analyzing the HEXRD spectrum, the weight fraction of the α_2
30 phase was determined to be 12.9 wt.% in the present as-HIPed alloy and is lower than
31 18 wt.% determined in the Ti-45Al-5Nb-0.75C alloy. This could explain a higher
32 volume fraction of the H-carbides found in the Ti-46Al-8Nb-0.7C alloy as a decrease
33 in the α_2 phase amount can promote the carbide formation [21]. In order to know
34 whether P-carbides have formed in the HIPed Ti-46Al-8Nb-0.7C alloy, the specimen
35 was further investigated by TEM.

36 The TEM images in Fig. 2 confirm the existence of the P-carbides in the HIPed
37 Ti-46Al-8Nb-0.7C alloy. P-carbides have formed at grain boundaries and interfaces,
38 at dislocations (Fig. 2a) and in the γ laths as well as the equiaxed γ grains (Fig. 2b).
39 All the P-carbides exhibit the orientation relationship $[001]_{\gamma} // [001]_{\text{P}}$ and $(100)_{\gamma} // (100)_{\text{P}}$

1 with the γ matrix. The precipitates in the γ grains have a well-reported needle-like
2 morphology with the long axis parallel to the $[001]_{\gamma}$ zone axis [23]. Thus, they show
3 dot-like cross-sections when viewed along the $[001]_{\gamma}$ direction as shown in Figs. 2b
4 and c. Additionally, “coffee-bean” contrast is visible around the carbides in Fig. 2b
5 due to the strain field caused by the coherent stress. As evidenced in Fig. 2c, the
6 interface between the γ matrix and the P-carbide is coherent. According to the
7 HEXRD investigation, the lattice parameters of the γ matrix and P-carbides are
8 $a_{\gamma}=0.402$ nm, $c_{\gamma}=0.408$ nm, and $a_p=0.415$ nm, respectively. The lattice misfit between
9 the P-carbides and the γ matrix along the $[001]_{\gamma}$ and $[100]_{\gamma}$ directions can be
10 calculated by the following equations: $\varepsilon_{100}=(a_p-a_{\gamma})/a_p$ and $\varepsilon_{001}=(a_p-c_{\gamma})/a_p$, indicating a
11 smaller lattice misfit of 1.7 % along the $[001]_{\gamma}$ orientation compared to 3.1 % along
12 the $[100]_{\gamma}$ direction. Therefore, the P-carbides in the γ matrix prefer to grow along the
13 $[001]_{\gamma}$ direction, forming a needle-like shape to reduce the misfit in the $[100]_{\gamma}$ and
14 $[010]_{\gamma}$ directions, which is in accordance with that reported in [23]. Previous studies
15 proved that P-carbides could be dissolved at temperatures above 1100 °C, indicating
16 that the observed P-carbides in the HIPed sample precipitated during the furnace
17 cooling [29].

18 19 **3.2 Creep test results**

20 The creep test results are shown in Fig. 3 and Table. 1. The creep time until failure is
21 850 h for the sample tested at 850 °C/260 MPa and 3267 h for the sample tested at
22 850 °C/130 MPa. The creep curve of the sample crept at 850 °C/130 MPa exhibits a
23 short primary creep stage and a long secondary creep stage. When the creep time
24 reaches 3200 h, a short accelerated tertiary creep stage is observed. The sample crept
25 at 750 °C/260 MPa has reached 8500 h without rupture. Table 2 summarizes the creep
26 properties of the high Nb-TiAl alloys reported in literature. It is found that the high
27 Nb-TiAl alloys with duplex microstructures show significantly lower creep resistance
28 and the alloys are easier to deform during creep [31]. The carbon containing TiAl
29 alloys have a longer creep life but smaller creep fracture strain than the carbon-free
30 alloys with similar compositions [5-7]. Compared with the results in Table 2, the
31 Ti-46Al-8Nb-0.7C alloy exhibits better creep resistance with a longer creep life but a
32 limited creep strain, which is, despite the creep strain, apparently superior to the
33 reported alloys with varied compositions.

34 In the following, the microstructure evolution during creep tests will be examined by
35 SEM, HEXRD and TEM in order to understand the influences of test conditions on
36 the microstructure and thus creep properties of the Ti-46Al-8Nb-0.7C alloy.

37 38 **3.3 Influences of stress and temperature on microstructure evolution**

3.3.1 SEM observation

Fig. 4 shows the microstructure of the samples crept at 850 °C. At this temperature, with increasing creep time, more and more carbides (both P- and H-types) form at different positions. Due to the large sizes, some coarsened P-carbides at grain boundaries can also be identified in the SEM images (for example at grain boundaries in Fig. 4f). After creep under 260 MPa for 110 h, in the gauge section (Fig. 4a) the α_2 laths in some lamellar colonies start to decompose via the “parallel decomposition” [28], resulting in the coarsening of neighboring γ laths. Besides, numerous needle- or plate-like precipitates with varied sizes are observed along the decomposed α_2 laths, which are H-carbides that form at the expense of the α_2 phase [21, 32-34]. In contrast, in the holder section (Fig. 4b), the α_2 laths do not change obviously, i.e. nearly no decomposition of the α_2 phase occurs. With extending creep time to 850 h and above, the α_2 lath decomposition in some lamellar colonies is more significant in the gauge section (Fig. 4c). Additionally, some lamellae are curved near grain boundaries and cavities form along the lamellar boundaries due to grain boundary sliding effects (Fig. 4d), which can initiate crack propagation along colony boundaries [9, 35, 36]. In the holder section, α_2 laths in some lamellar colonies also decompose and H-carbides form and consume the α_2 phase (Fig. 4e). However, no curved lamellae or cavities are observed (Fig. 4f). The difference in microstructure evolution between the gauge and holder sections should be due to the different stress conditions in the two sections. At a short creep time (110 h), in the gauge section the α_2 laths tend to decompose due to the applied stress while in the holder section where the stress should be nearly absent, the α_2 laths are relatively thermally stable. With continuing creep to 850 h, the α_2 laths in the holder section also start to decompose, as they are not thermodynamically stable at this temperature.

The thermal stability of the α_2 laths is higher under a smaller stress of 130 MPa. After creep for 1100 h, the α_2 laths in the lamellar colonies only show a slight decomposition (Fig. 4g). After further creep until fracture for the extended period of 3267 h, the α_2 laths in the lamellar colonies decompose significantly with formation of numerous H-carbides at the expense of the α_2 phase (Fig. 4h). In addition, the lamellae are severely deformed (curved and broken) and numbers of fine equiaxed γ grains in sizes of less than 10 μm form at the lamellar boundaries. Previous studies hint that the equiaxed γ grains with fine grain size could deteriorate the creep resistance [11-13]. Compared to the limited width of the γ laths, dislocation gliding in the equiaxed γ grains can be easier since there is more free space in various directions. However, the glide distance of dislocations in these γ grains is still limited because of the small grain sizes. As a result, stress can be accumulated at the grain boundaries. Together with the carbide precipitation at the boundary, the initiation of cracks is prone to happen in the positions where coarse carbides appear. Moreover, the

1 increased grain boundary surface also facilitates grain boundary gliding, leading to the
2 formation of cavities. In fact, the cracks along the lamellar colony boundaries are
3 commonly observed in the failed creep samples.

4 The lamellar microstructures in the gauge section of the samples crept at 750 °C under
5 130 and 260 MPa for 1200 h are shown in Fig. 5. It is found that the α_2 laths are also
6 stable at a lower temperature. Again, with increasing stress, α_2 laths decompose more
7 significantly and more H-carbides form at the primary α_2 lath position. Thus, from the
8 above results, it can be concluded that the creep temperature and stress can strongly
9 influence the stability of the lamellar structure. A higher creep temperature and stress
10 can promote the α_2 lath decomposition, resulting in the formation of the H-carbides at
11 their locations at the expense of α_2 phase.

12 13 **3.3.2 HEXRD investigations**

14 Fig. 6 shows the HEXRD spectrums for the creep specimens tested at different
15 conditions. The microstructure is mainly composed of the γ phase with a weight
16 fraction of around 90-95%. The fraction of α_2 phase is reduced compared to that in the
17 HIPed state and the detailed values in the holder section at different creep conditions
18 are listed in Table 3. The results show that the α_2 phase fraction decreases with
19 increasing creep temperature and time due to continuous $\alpha_2 \rightarrow \gamma + \text{H-carbide}$ phase
20 transformation during the creep process. This phenomenon has also been found in a
21 former study in the Ti-45Al-5Nb-0.5/0.75C alloys after annealing at different
22 temperatures and times [21]. From Figs. 4 and 5 it is clearly shown that an increase in
23 creep stress promotes the decomposition of the α_2 laths in the gauge section. Thus, by
24 increasing creep temperature, stress and time, the α_2 laths decompose more
25 significantly, resulting in the γ lath coarsening and the formation of H-carbides at the
26 expense of the α_2 phase.

27 The fractions of the P- and H-carbides could not be determined using the Rietveld
28 analysis that was applied to calculate the α_2 phase fraction due to their small contents.
29 A rough estimation on the carbide fraction evolution when altering the creep time,
30 stress and temperature can be made based on the change on the intensity of the
31 carbide reflections. For this, it is assumed that the γ phase is the majority phase and its
32 fraction remains the same when test parameters change. In Fig. 6, all the HEXRD
33 spectrums were normalized to the highest reflection $\{111\}_\gamma$. For the specimen crept
34 850 °C and 260 MPa for 110 h, the P-carbide fraction shows no clear difference in the
35 holder and gauge sections as the intensity of the $\{111\}_P$ and $\{200\}_P$ peaks in these two
36 sections is similar. While, the fraction of the H-carbides is obviously higher in the
37 gauge section than in the holder section due to a high intensity of the $\{106\}_H$ peak in
38 the gauge section. This agrees with the SEM observation in Figs. 4a and b that the α_2
39 laths decompose and H-carbides form in the gauge section. After creep at 850 °C and

1 130 MPa for 1100 h, the fractions of the P- and H-carbides did not vary a lot in the
2 holder and gauge sections indicated by the similar intensity of the carbide reflections.
3 This hints that the stress condition difference between the holder and gauge sections
4 did not influence the precipitation of the P- and H-carbides after a very long creep
5 time. In addition, it is found that the volume fractions of the P- and H-carbides in the
6 specimen after creep at 850 °C and 130 MPa for 1100 h are much higher than those in
7 the specimen after creep at 850 °C and 260 MPa for 110 h as can be concluded from
8 the higher carbide peak intensity in the former alloy. This seems to contradict the
9 SEM observation that more α_2 laths are found to decompose and more H-carbides
10 form in the lamellar colonies in the specimen crept for 110 h. However, it should be
11 kept in mind that carbides also form in the γ matrix, at interfaces and grain boundaries
12 that account for the majority of the carbide fraction. Thus, it can be concluded that the
13 carbides form and grow continuously with increasing creep time and the carbide
14 precipitation might not reach the thermodynamically equilibrium condition even after
15 creep for 1100 h. At a lower creep temperature of 750 °C, the P-carbide fraction also
16 does not vary a lot in the holder and gauge sections when the creep stress is changed
17 as a similar intensity is found for the $\{111\}_P$ or $\{200\}_P$ peak. While, the fraction of the
18 H-carbides is always higher in the gauge sections of the specimens under a higher
19 creep stress due to the larger amount of α_2 lath decomposition as shown in Fig. 5.
20 Compared with the situation after creep at 850 °C, the influence of the stress on the
21 formation of H-carbides is found after creep for 1200 h at 750 °C. It could be inferred
22 that this influence will be eliminated after a longer creep time when the precipitation
23 of the carbides gets close to the thermodynamic equilibrium condition. With respect to
24 the influence of the creep temperature on carbide formation, the spectrums tested at
25 the same creep stress and for a similar time, i.e. at 850 °C, 130 MPa, 1100 h and at
26 750 °C, 130 MPa, 1200 h, are compared. It is found that both the P- and H-carbide
27 fractions increase with creep temperature as the $\{111\}_P$, $\{200\}_P$ and $\{106\}_H$ peak
28 intensities are higher at 850 °C. Thus, a higher creep temperature promotes the
29 formation of both P- and H-carbides due to a smaller α_2 phase fraction at a higher
30 temperature.

31 32 **3.3.3 TEM observation of carbide formation during creep**

33 As shown in the above results, P-carbides have already formed at dislocations, at
34 interfaces and grain boundaries, and in the γ phase in the HIPed state. With further
35 annealing during creep, more P-carbides would form at these locations. Compared to
36 the coarse H-carbides, P-carbides commonly have smaller sizes. Fig. 7 shows the
37 P-carbide precipitation in specimens crept at 750 °C for 1200 h. As already known
38 from the HEXRD results, the creep stress has no obvious influence on the P-carbide
39 fraction. Also in the TEM observation, the distribution and morphology evolution of

1 the P-carbides was found to be similar for different creep stresses. As shown in Figs.
2 7a-c, after creep at 750 °C for 1200 h, numerous P-carbides are present at dislocations,
3 at lamellar interfaces, in the γ laths and in equiaxed γ grains. However, the
4 deformation seems not severe in the γ phase after creep for 1200 h as only few
5 dislocations are found. With further creep deformation, it is expected that the
6 P-carbides can efficiently hinder the dislocation glide in the γ phase and thus
7 contribute to a long creep life of the alloy. Additionally, the morphology of P-carbides
8 in the γ phase has changed from needles into conglomerates of small sub-particles by
9 splitting. The conglomerates of sub-particles resemble a plate-like morphology with
10 the plate planes parallel to the $(100)_{\gamma}$ and $(010)_{\gamma}$ crystallographic planes. So when
11 viewed along the $\langle 100 \rangle_{\gamma}$ orientation, two sets of carbide conglomerate projections are
12 observed as shown in the insert in Fig. 7d. The needle-like projections belong to the
13 carbide conglomerates with the plate plane parallel to the $(010)_{\gamma}$ crystallographic
14 plane and the plate-like projections are from those with the plate plane parallel to the
15 $(100)_{\gamma}$ crystallographic plane. The needle-like projection in Fig. 7d is composed of
16 P-carbide sub-particles and the interspersed γ phase (γ_i) whose orientation has a 90°
17 deviation from that of the surrounding γ matrix. While, the atomic arrangement differs
18 among the P-carbides, the γ_i phase and the γ matrix are hardly discernible in the
19 plate-like projection (Fig. 7e) as also found in our previous study [22]. This could be
20 probably due to the small thickness of the carbide conglomerate, thus information
21 comes from the carbide conglomerate and the γ matrix located above or below it.
22 Viewing long the $[001]_{\gamma}$ orientation, cross-sections are observed to have regions of
23 sub-carbide particles and the γ_i phase with an orientation 90° rotated with respect to
24 the surrounding γ matrix. The carbide splitting phenomenon has also been found in
25 the Ti-45Al-5Nb-(0.5-1)C alloys during annealing at 800 and 900 °C [20-22]. This
26 suggests that the applied external stress shows no obvious influence on the
27 morphology development of the P-carbides.

28 At a higher creep temperature of 850 °C under 260 MPa for 110 h, the interaction
29 between the dislocations and P-carbides greatly increases, as shown in Fig. 8a. The
30 dislocations are strongly pinned by the P-carbides densely nucleated along the
31 dislocations and thus the creep resistance of the alloy should be improved by the
32 precipitation strengthening mechanism [7, 15]. In addition, P-carbides in the γ phase
33 are also observed to split (Fig. 8b). With further creep for 850 h, the P-carbides in the
34 γ phase have disappeared and only a few P-carbides exist at dislocations and lamellar
35 interfaces (Fig. 8c). Instead, more coarse P-carbides are found at grain boundaries.
36 Compared to the situation at 750 °C, the P-carbides in the γ grain interior are less
37 stable at 850 °C. Figs. 8d-e show the carbide precipitates in the specimens creep under
38 130 MPa for 1100 and 3267 h, respectively. After creep for 1100 h, only a few
39 P-carbides are found at dislocations in the γ phase and at the lamellar interfaces. A

1 redistribution of carbon from small carbides in the γ grain interior to large carbides at
2 grain boundaries happens. Therefore, the carbon has mostly concentrated in the coarse
3 carbides in sizes of tens to hundreds of nanometers after long-term creep [21, 29].
4 In SEM observation, elongated H-carbides are always found to form at the α_2 lath
5 positions. This precipitation process should be induced by the dissolution of the α_2
6 laths during creep. Fig. 9 shows such H-carbides pictured by HRTEM. In Fig. 9a, a
7 coarse H-carbide with long-periodic structure seems to nucleate at the α_2/γ interface
8 and grows at the expense of not only the α_2 lath but also the γ laths at both sides.
9 These three phases follow the orientation relationships: $[101]_\gamma//[11\bar{2}0]_H//[11\bar{2}0]_{\alpha_2}$ and
10 $(11\bar{1})_\gamma/(0006)_H/(0002)_{\alpha_2}$. The interface between the H-carbide and the α_2 phase is
11 determined to be coherent while it is semi-coherent between the H-carbide and the γ
12 phase as evidenced by the ledges at the interfaces. This can be explained by the lattice
13 mismatch between these phases. According to the HEXRD results of this specimen,
14 the lattice parameters are determined to be $a=0.578$ and $c=0.466$ nm for the α_2 phase,
15 $a=0.402$ and $c=0.408$ nm for the γ phase, and $a=0.305$ and $c=1.374$ nm for the H
16 phase. Then, the lattice mismatch is calculated to be $\frac{d_{(0002)\alpha_2}-d_{(0006)H}}{d_{(0002)\alpha_2}} = \frac{0.231-0.229}{0.231} =$
17 0.9% between the $(0002)_{\alpha_2}$ and $(0006)_H$ planes and $\frac{d_{(11\bar{1})\gamma}-d_{(0006)H}}{d_{(11\bar{1})\gamma}} = \frac{0.233-0.229}{0.233} =$
18 1.7% between the $(11\bar{1})_\gamma$ and $(0006)_H$ planes. Thus, a smaller lattice mismatch exists
19 between the H-carbide and the α_2 phase, and the small thickness of the α_2 lath also
20 contributes to a coherent H- α_2 interface. It is also occasionally found that H-carbides
21 precipitate within the γ laths with the above mentioned orientation relationship:
22 $[101]_\gamma/[11\bar{2}0]_H$ and $(11\bar{1})_\gamma/(0006)_H$ as shown in Fig. 9b. It should be noted that the
23 decomposition of α_2 lath proceeds with creep. Nano-sized fine α_2/γ lamellar structures
24 are commonly found in long-term crept samples (Fig. 9c). As reported in literature [37,
25 38], the decomposition of α_2 laths is inevitable during long-term thermal exposure as
26 well as in crept samples in different TiAl-based alloys, whereas in the present alloy
27 this process is largely slowed down due to the stabilization of α_2 phase with carbon.
28 Combining the SEM, HEXRD and TEM results, the influences of the creep
29 temperature, stress and time on the microstructure and carbide precipitation can be
30 concluded as follows. With increasing the creep temperature and stress, the
31 decomposition of the α_2 laths is more pronounced and the precipitation of H-carbides
32 at the expense of the α_2 phase occurs at the γ/α_2 interfaces. With increasing creep time,
33 the microstructure gets closer to thermodynamic equilibrium condition and the
34 volume fraction of the α_2 phase is reduced accordingly. With respect to carbide
35 precipitation, the volume fraction of carbides increases with creep temperature and
36 time. While, the thermal stability of the P-carbides in the γ phase is reduced and
37 redistribution of carbon from the small carbides in grain interior to the large carbides

1 at grain boundaries occurs in a shorter creep time with increasing creep temperature.
2 The creep stress plays no obvious role in the precipitation and morphology
3 development of the P-carbides but influences greatly the formation of the H-carbides
4 at γ/α_2 interfaces by affecting the stability of the α_2 laths in lamellar colonies.

6 **3.4 Influence of carbon and microstructure on creep resistance**

7 Based on the above results, the Ti-46Al-8Nb-0.7C alloy exhibits good creep
8 resistance. To the authors' knowledge, the creep property of this alloy is one of the
9 best reported for polycrystalline TiAl alloys with nearly lamellar structure [39]. This
10 can be attributed to the following factors. Firstly, high-Nb TiAl alloys are considered
11 to have high strength because of the solid solution effect of Nb and C atoms, causing
12 a higher critical stress to activate dislocations [40, 41]. Secondly, in the primary creep
13 stage, the nearly fully lamellar microstructure has good thermal stability and the
14 addition of carbon can further stabilize the α_2 phase and hinder the formation of β_0
15 and ω_0 phases [18]. As creep cavities tend to form along the grain boundaries of
16 equiaxed γ grains rather than within the lamellar colonies [35, 36], the good
17 microstructural stability can contribute to the good creep resistance by reducing the
18 formation of equiaxed γ grains. Thirdly, the precipitation of the P-carbides at
19 dislocations in the γ phase can pin the dislocations and strongly slow down and hinder
20 their glide. The closely distributed P-carbides at the lamellar interfaces could also
21 play a role in preventing the activation of bow-out interface dislocations under stress
22 [39]. Compared to smaller and densely dispersed P-carbides, H-type carbides in the γ
23 phase might be less beneficial for improving creep properties. However, for the
24 H-carbides distributing along the γ/α_2 interfaces, a number of studies reported that
25 they were beneficial for creep resistance because the elongated H-carbides acted as
26 hard-phase islands to preserve the γ/α_2 interfaces and restrict the movement of
27 interfacial dislocations [32-34]. Recent investigations also reported that the random
28 primary H-carbides could enhance the fracture toughness and creep resistance of
29 carbon containing high Nb-TiAl alloys by restraining the crack propagation [24, 42].
30 Thus, the precipitation of H-carbides at the γ/α_2 interfaces is supposed to contribute to
31 a better creep resistance of the Ti-46Al-8Nb-0.7C alloy. As the creep proceeds, more
32 and more fine P-carbides precipitate in the γ phase. However, there should be a
33 certain moment when the supersaturation of the γ phase with C is exhausted by
34 carbide precipitation. Then the coarsening of carbides and redistribution of carbon to
35 large grain boundary carbides have become the main trends of microstructure
36 evolution. As a result, the pinning effect on dislocations starts to decrease. This can be
37 a very long period since even in the samples after 1100 h creep the carbides can still
38 be observed in γ grain interior. In the third stage of creep, the coarse carbides may
39 have limited effect on the pinning of dislocations. Therefore, the dislocations would

1 have more free space to glide without obstacles. Moreover, the decomposition of α_2
2 phase introduces numerous new lamellar interfaces, which further provide extra
3 dislocation sources and more volume of deformable γ phase free of carbides. However,
4 it should be noted that the overall ductilities of the creep samples are all very low (less
5 than 3%), meaning that the dislocation movement cannot be comprehensively
6 activated in the whole sample. The recrystallized γ grains at the lamellar colony
7 boundaries could contribute to the overall deformation. But this can only be effective
8 after long-term annealing. Additionally, the newly formed γ grains at lamellar colony
9 boundaries would also contribute to grain boundary gliding. This can explain the
10 sudden increase of the strain rate in the last section of the creep curve. The difference
11 in the creep life of the samples deformed at 750 and 850 °C possibly comes from the
12 dislocation climb mechanism, which is less active at lower temperatures.

14 4. Conclusions

15 In this study, the creep properties and the effects of creep temperature, stress and time
16 on the microstructural evolution and carbide precipitation in a high Nb-TiAl alloy are
17 investigated during creep at intermediate temperatures. The main results are
18 concluded as follows.

- 19 (1) The Ti-46Al-8Nb-0.7C alloy exhibits good creep resistance and the creep life is
20 850 h and 3267 h for samples crept at 850 °C/260 MPa and 850 °C/130 MPa,
21 respectively. The creep life of the sample crept at 750 °C and 260 MPa is more
22 than 8500 h without rupture.
- 23 (2) The Ti-46Al-8Nb-0.7C alloy shows good microstructural stability during creep at
24 intermediate temperatures. The microstructure is slightly decomposed by
25 formation of equiaxed γ grains at the lamellar boundaries and the decomposition
26 of α_2 laths which is more obvious at higher creep temperature and stress.
- 27 (3) Numerous P-carbides precipitate in the γ laths and equiaxed γ grains, which can
28 hinder the dislocation motion and thus improve the creep resistance. The
29 decomposition of the α_2 laths induced H-carbide precipitation at the γ/α_2 lamellar
30 interfaces. The interfacial H-carbides can preserve the γ/α_2 interfaces and restrict
31 the movement of interfacial dislocations, and thus improve the creep resistance.
- 32 (4) The volume fraction of carbides increases with creep temperature and time.
33 However, the creep stress hardly affects the precipitation and morphology
34 development of the P-carbides but a higher stress can promote the precipitation of
35 H-carbides at γ/α_2 interfaces by destabilizing the α_2 laths in the lamellar colonies.

37 Acknowledgments

38 This work was supported by the National Natural Science Foundation of China
39 (contract No. 51601146), State Key Lab of Advanced Metals and Materials (contract

1 No. 2017-ZD02), and Natural Science Basic Research Plan of Shaanxi Province
2 (contract No. 2017JQ5006). Li Wang acknowledges the financial support from the
3 Helmholtz Association in the frame of Helmholtz Postdoc Program. Lin Song
4 acknowledges the fruitful discussion with Dr. J.D.H. Paul and his help on the creep
5 tests.

6 7 **References**

8 [1] Y.W. Kim, S.L. Kim, Advances in Gammalloy Materials-Processes-Application
9 Technology: Successes, Dilemmas, and Future, JOM (2018).

10 [2] H. Clemens, S. Mayer, Design, Processing, Microstructure, Properties, and Applications
11 of Advanced Intermetallic TiAl Alloys, Adv. Eng. Mater. 15 (2013) 191-215.

12 [3] H. Clemens, H. Kestler, Processing and Applications of Intermetallic γ - TiAl- Based
13 Alloys, Adv. Eng. Mater. 2 (2000) 551-570.

14 [4] F. Appel, U. Brossmann, U. Christoph, S. Eggert, P. Janschek, U. Lorenz, J. Müllauer, M.
15 Oehring, J.D.H. Paul, Recent Progress in the Development of Gamma Titanium Aluminide
16 Alloys, Adv. Eng. Mater. 2 (2000) 699-720.

17 [5] R. Chen, Q. Wang, Y. Yang, J. Guo, Y. Su, H. Ding, H. Fu, Brittle–ductile transition during
18 creep in nearly and fully lamellar high-Nb TiAl alloys, Intermetallics 93 (2018) 47-54.

19 [6] M. Kasthuber, B. Rashkova, H. Clemens, S. Mayer, Enhancement of creep properties
20 and microstructural stability of intermetallic β -solidifying γ -TiAl based alloys, Intermetallics
21 63 (2015) 19-26.

22 [7] Y.W. Kim, S.L. Kim, Effects of microstructure and C and Si additions on elevated
23 temperature creep and fatigue of gamma TiAl alloys, Intermetallics 53 (2014) 92-101.

24 [8] T. Klein, L. Usategui, B. Rashkova, M.L. Nó, J.S. Juan, H. Clemens, S. Mayer,
25 Mechanical behavior and related microstructural aspects of a nano-lamellar TiAl alloy at
26 elevated temperatures, Acta Mater. 128 (2017) 440-450.

27 [9] W. Qi, R. Chen, G. Xue, J. Guo, Y. Su, H. Ding, H. Fu, Microstructure control and creep
28 behavior of Ti-47Al-6Nb-0.1C alloy by directional solidification, Intermetallics 94 (2018)
29 152-159.

30 [10] H. Zhu, D.Y. Seo, K. Maruyama, P. Au, Effect of microstructural stability on creep
31 behavior of 47XD TiAl alloys with fine-grained fully lamellar structure, Scripta Mater. 52
32 (2005) 45-50.

33 [11] M. Kasthuber, B. Rashkova, H. Clemens, S. Mayer, Effect of microstructural
34 instability on the creep resistance of an advanced intermetallic γ -TiAl based alloy,
35 Intermetallics 80 (2017) 1-9.

36 [12] S. Karthikeyan, M.J. Mills, The role of microstructural stability on compression creep of
37 fully lamellar γ -TiAl alloys, Intermetallics 13 (2005) 985-992.

38 [13] H. Zhu, D.Y. Seo, K. Maruyama, Effect of lamellar spacing on microstructural instability
39 and creep behavior of a lamellar TiAl alloy, Scripta Mater. 54 (2006) 1979-1984.

40 [14] W.H. Tian, M. Nemoto, Effect of carbon addition on the microstructures and mechanical
41 properties of γ -TiAl alloys, Intermetallics 5 (1997) 237-244.

42 [15] E. Schwaighofer, B. Rashkova, H. Clemens, A. Stark, S. Mayer, Effect of carbon
43 addition on solidification behavior, phase evolution and creep properties of an intermetallic

- 1 β -stabilized γ -TiAl based alloy, *Intermetallics* 46 (2014) 173-184.
- 2 [16] F. Appel, U. Christoph, R. Wagner, Solution and Precipitation Hardening in
3 Carbon-Doped Two-Phase γ -Titanium Aluminides, *Mrs Proceedings* 460 (1996) 77.
- 4 [17] U. Christoph, F. Appel, R. Wagner, Dislocation dynamics in carbon-doped titanium
5 aluminide alloys, *Mater. Sci. Eng. A* 239-240 (1997) 39-45.
- 6 [18] T. Klein, M. Schachermayer, F. Mendez-Martin, T. Schöberl, B. Rashkova, H. Clemens,
7 S. Mayer, Carbon distribution in multi-phase γ -TiAl based alloys and its influence on
8 mechanical properties and phase formation, *Acta Mater.* 94 (2015) 205-213.
- 9 [19] H.S. Park, S.W. Nam, N.J. Kim, S.K. Hwang, Refinement of the lamellar structure in
10 TiAl-based intermetallic compound by addition of carbon, *Scripta Mater.* 41 (1999)
11 1197-1203.
- 12 [20] J. Lapin, T. Pelachová, O. Bajana, High temperature deformation behaviour and
13 microstructure of cast in-situ TiAl matrix composite reinforced with carbide particles, *J. Alloy.*
14 *Compd.* 797 (2019) 754-765.
- 15 [21] L. Wang, U. Lorenz, M. Münch, A. Stark, F. Pyczak, Influence of alloy composition and
16 thermal history on carbide precipitation in γ -based TiAl alloys, *Intermetallics* 89 (2017)
17 32-39.
- 18 [22] L. Wang, M. Oehring, U. Lorenz, A. Stark, F. Pyczak, New insights into perovskite-Ti₃
19 AlC precipitate splitting in a Ti-45Al-5Nb-0.75C alloy by transmission electron microscopy,
20 *Intermetallics* 100 (2018) 70-76.
- 21 [23] L. Wang, C. Zenk, A. Stark, P. Felfer, H. Gabrisch, M. Göken, U. Lorenz, F. Pyczak,
22 Morphology evolution of Ti₃AlC carbide precipitates in high Nb containing TiAl alloys, *Acta*
23 *Mater.* 137 (2017) 36-44.
- 24 [24] J. Lapin, K. Kamyshnykova, Processing, microstructure and mechanical properties of
25 in-situ Ti₃Al+TiAl matrix composite reinforced with Ti₂AlC particles prepared by centrifugal
26 casting, *Intermetallics* 98 (2018) 34-44.
- 27 [25] X. Hu, J. Li, L. Song, T. Zhang, Coupling effects of deformation and thermal exposure
28 on the precipitation behaviors of $\beta_0(\omega)$ phases in a high Nb-containing TiAl alloy, *Mater. Des.*
29 148 (2018) 135-144.
- 30 [26] L. Song, L.Q. Zhang, X.J. Xu, J. Sun, J.P. Lin, Omega phase in as-cast
31 high-Nb-containing TiAl alloy, *Scripta Mater.* 68 (2013) 929-932.
- 32 [27] Z.W. Huang, Thermal stability of Ti-44Al-4Nb-4Zr-0.2Si-1B alloy, *Intermetallics* 42
33 (2013) 170-179.
- 34 [28] Z.W. Huang, D.G. Zhu, Thermal stability of Ti-44Al-8Nb-1B alloy, *Intermetallics* 16
35 (2008) 156-167.
- 36 [29] L. Wang, H. Gabrisch, U. Lorenz, F.P. Schimansky, A. Schreyer, A. Stark, F. Pyczak,
37 Nucleation and thermal stability of carbide precipitates in high Nb containing TiAl alloys,
38 *Intermetallics* 66 (2015) 111-119.
- 39 [30] H. Gabrisch, A. Stark, F.P. Schimansky, L. Wang, N. Schell, U. Lorenz, F. Pyczak,
40 Investigation of carbides in Ti-45Al-5Nb-xC alloys ($0 \leq x \leq 1$) by transmission electron
41 microscopy and high energy-XRD, *Intermetallics* 33 (2013) 44-53.
- 42 [31] T. Ye, L. Song, S. Gao, Y. Liang, Y. Wang, J. Lin, Precipitation behavior of the ω_0 phase
43 in an annealed high Nb-TiAl alloy, *J. Alloy. Compd.* 701 (2017) 882-891.
- 44 [32] P.I. Gouma, K. Subramanian, Y. W. Kim, M. J. Mills, Annealing studies of γ -titanium

- 1 aluminides alloyed with light elements for creep strengthening, *Intermetallics* 6 (1998)
2 689-693.
- 3 [33] P.I. Gouma, M. J. Mills, Characterization of the precipitation process in a TiAl-based
4 alloy with carbon and silicon additions, *Philos. Mag. Lett.* 78 (1998) 59-66.
- 5 [34] M. Karadge, P. I. Gouma, Y. W. Kim, Precipitation strengthening in K5-series γ -TiAl
6 alloyed with silicon and carbon, *Metall. Mater. Trans. A* 34 (2003) 2129-2138.
- 7 [35] X.W. Du, J. Zhu, Y.W. Kim, Microstructural characterization of creep cavitation in a
8 fully-lamellar TiAl alloy, *Intermetallics* 9 (2001) 0-146.
- 9 [36] M.E. Kassner, T.A. Hayes, Creep cavitation in metals, *Int. J. Plasticity* 19 (2003)
10 1715-1748.
- 11 [37] Z.W. Huang, T. Cong, Microstructural instability and embrittlement behaviour of an
12 Al-lean, high-Nb γ -TiAl-based alloy subjected to a long-term thermal exposure in air,
13 *Intermetallics* 18 (2010) 161-172.
- 14 [38] S. Bystrzanowski, A. Bartels, H. Clemens, R. Gerling, F.P. Schimansky, G. Dehm, H.
15 Kestler, Creep behaviour and related high temperature microstructural stability of
16 Ti-46Al-9Nb sheet material, *Intermetallics* 13 (2005) 515-524.
- 17 [39] F. Appel, J.D.H. Paul, M. Oehring, Creep, in: *Gamma Titanium Aluminide Alloys*,
18 Wiley-VCH Verlag GmbH & Co. KGaA, 2011 pp. 313-356.
- 19 [40] F. Appel, M. Oehring, R. Wagner, Novel design concepts for gamma-base titanium
20 aluminide alloys, *Intermetallics* 8 (2000) 1283-1312.
- 21 [41] G.E. Bean, M.S. Kesler, M.V. Manuel, Effect of Nb on phase transformations and
22 microstructure in high Nb titanium aluminides, *J. Alloy. Compd.* 613 (2014) 351-356.
- 23 [42] J. Lapin, A. Klimová, Z. Gabalcová, T. Pelachová, O. Bajana, M. Štamborská,
24 Microstructure and mechanical properties of cast in-situ TiAl matrix composites reinforced
25 with $(\text{Ti,Nb})_2\text{AlC}$ particles, *Mater. Des.* 133 (2017) 404-415.

Highlights

- Excellent creep properties are obtained in the Ti-46Al-8Nb-0.7C alloy
- Dislocations are pinned by P-carbides precipitated in the γ phase
- The volume fraction of carbides increases with creep temperature and time
- The stress hardly affects P-carbide evolution but promote H-carbide formation

Table 1 The creep test results in the Ti-46Al-8Nb-0.7C alloy

Temperature	stress	Time	strain	state
850 °C	260 MPa	850 h	1.7 %	rupture
850 °C	130 MPa	3267 h	3.0 %	rupture
750 °C	260 MPa	> 8500 h	> 1.3 %	unfaulted
750 °C	130 MPa	> 1200 h	> 0.2 %	unfaulted

Table 2 The creep properties of TiAl alloys with varied compositions reported in the literature

Composition (at.%)	Microstructure	Parameters	Creep time	Creep strain	Refs
Ti-45Al-8.5Nb-0.2W-0.2B-0.02Y	Duplex	850 °C, 130 MPa	68 h	27%	[3]
Ti-44Al-8Nb-0.2W-0.2B-0.1Y	NFL	800 °C, 200 MPa	147 h	6.0 %	[4]
Ti-44Al-6Nb-1Cr-2V	NFL	800 °C, 150 MPa	~600 h	~20 %	[5]
Ti-43.5Al-4Nb-1Mo-0.1B	NFL	815 °C, 150 MPa	~120 h	~6.2 %	[6]
Ti-43Al-4Nb-1Mo-0.1B-0.3C-0.3Si	NFL	815 °C, 150 MPa	~210 h	~3.0 %	[6]
Ti-46Al-3Nb-2Cr-0.2W	FL	760 °C, 276 MPa	138 h	1.4 %	[7]
Ti-46Al-3Nb-2Cr-0.2W-0.2Si-0.2C	FL	760 °C, 276 MPa	125 h	1.3 %	[7]
Ti-44Al-6Nb-1Cr-2V	NFL	800 °C, 276 MPa	~50 h	~21%	[8]
Ti-47Al-6Nb-0.1C	FL	800 °C, 276 MPa	~160 h	~5.0 %	[8]
Ti-47Al-6Nb-0.1C	FL	800 °C, 200 MPa	850 h	~6.0 %	[9]

Table 3 The α_2 phase fraction in the holder section of the crept samples after testing at different conditions. The α_2 phase fraction in the HIPed sample is also shown for comparison

Creep conditions	α_2 phase fraction, wt.%
HIPed state	12.9
@ 750 °C, 130 MPa, 1200 h	9.2
@ 850 °C, 130 MPa, 1100 h	8.0
@ 850 °C, 130 MPa, 3267 h	6.5
@ 850 °C, 260 MPa, 110 h	8.3
@ 850 °C, 260 MPa, 850 h	4.5

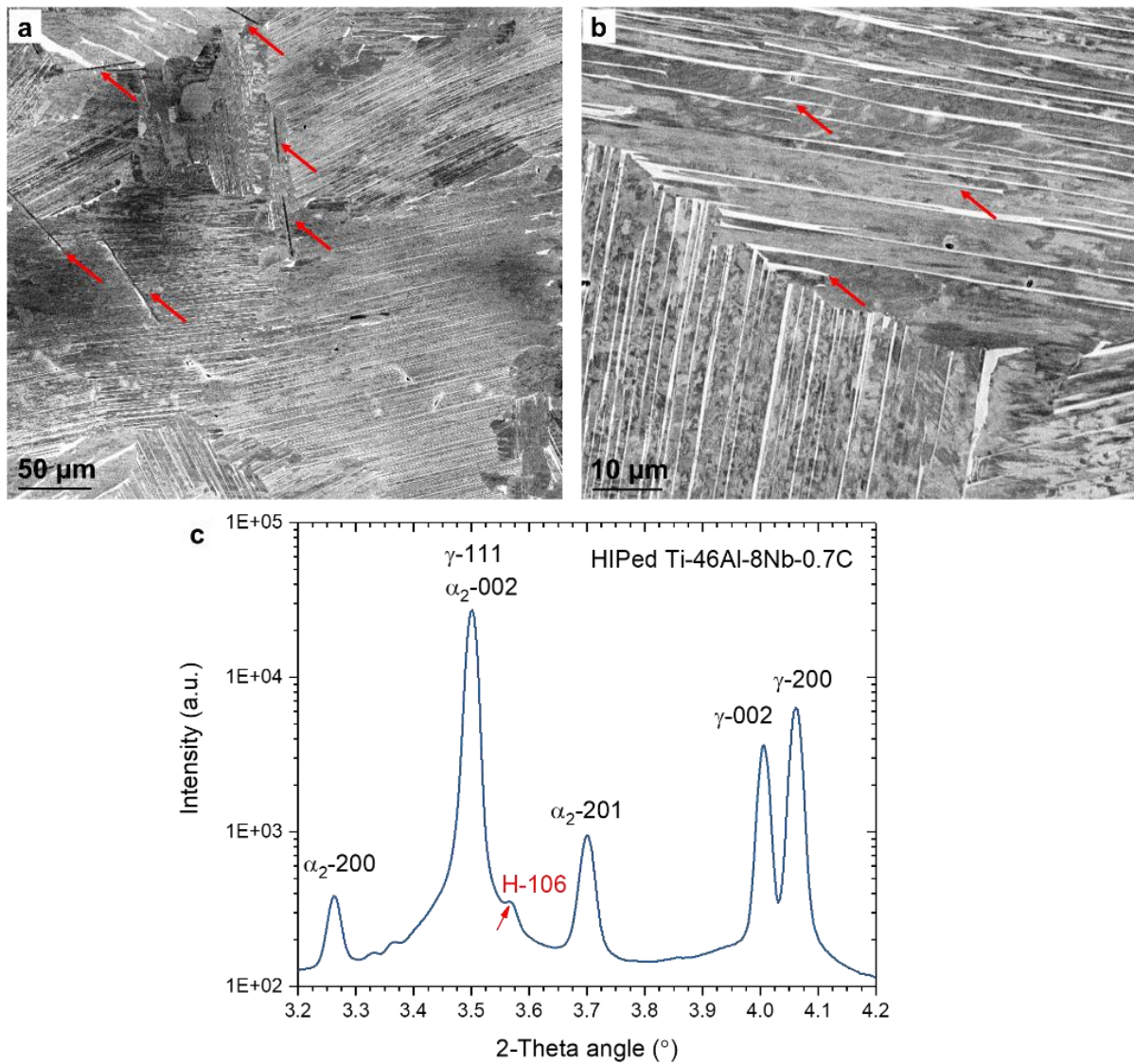


Fig. 1 Microstructure and phase constitution of the as-HIPed sample. (a, b) SEM images in back-scattered electron mode (the arrows in (a) and (b) indicate the locations of the H-carbides and the fractured α_2 laths, respectively); (c) HEXRD spectrum, the {106} peak of H-carbides is observed

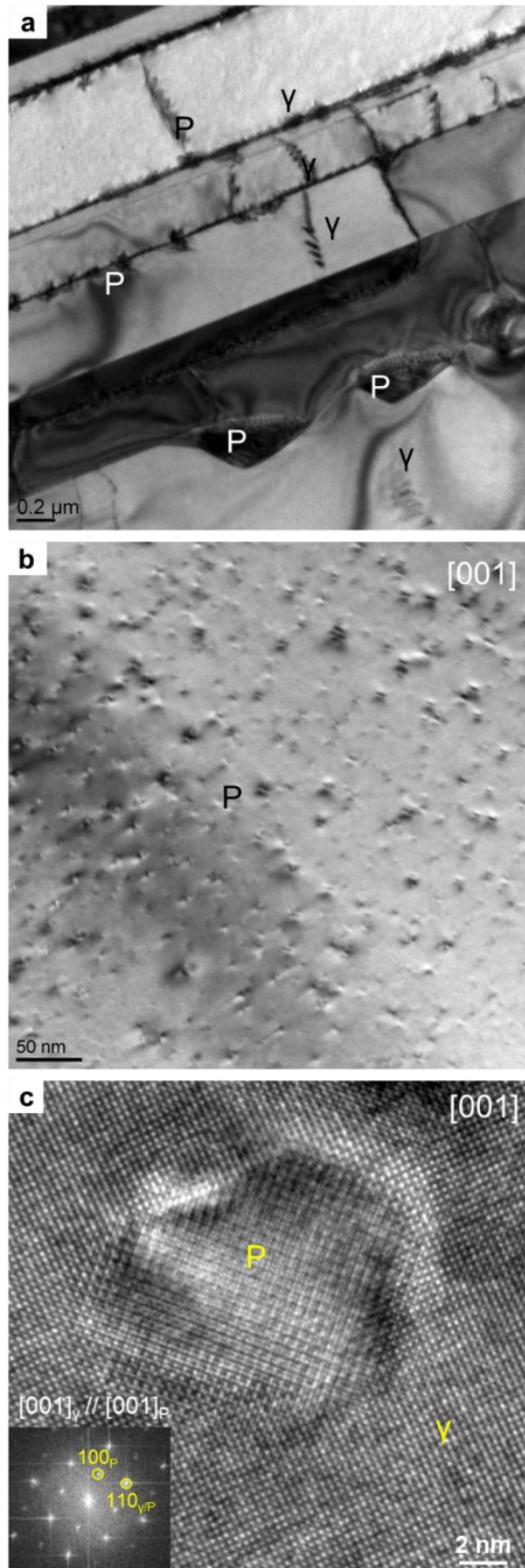


Fig. 2 TEM investigations on the distribution of P-carbides in the as-HIPed sample. (a) P-carbides exist at boundaries, γ twin interfaces and at dislocations, (b) in the γ matrix and (c) P-phase at atomic resolution imaged along the $[001]_{\gamma}$ zone axis

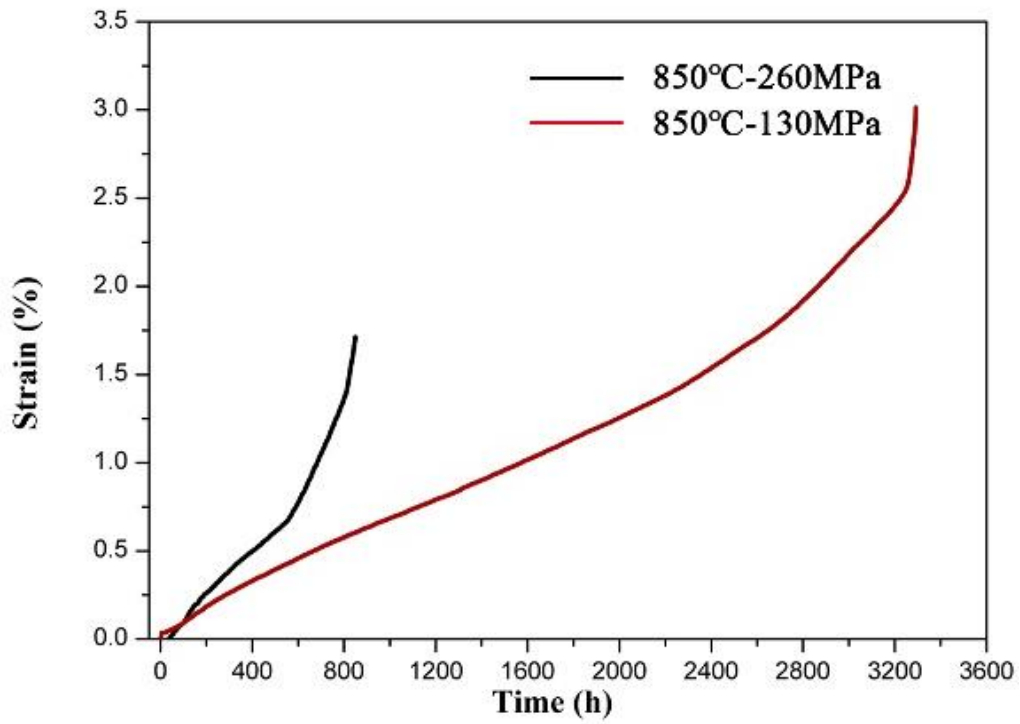


Fig. 3 Creep curves of the samples tested at 850 °C under tensile stresses of 130 and 260 MPa

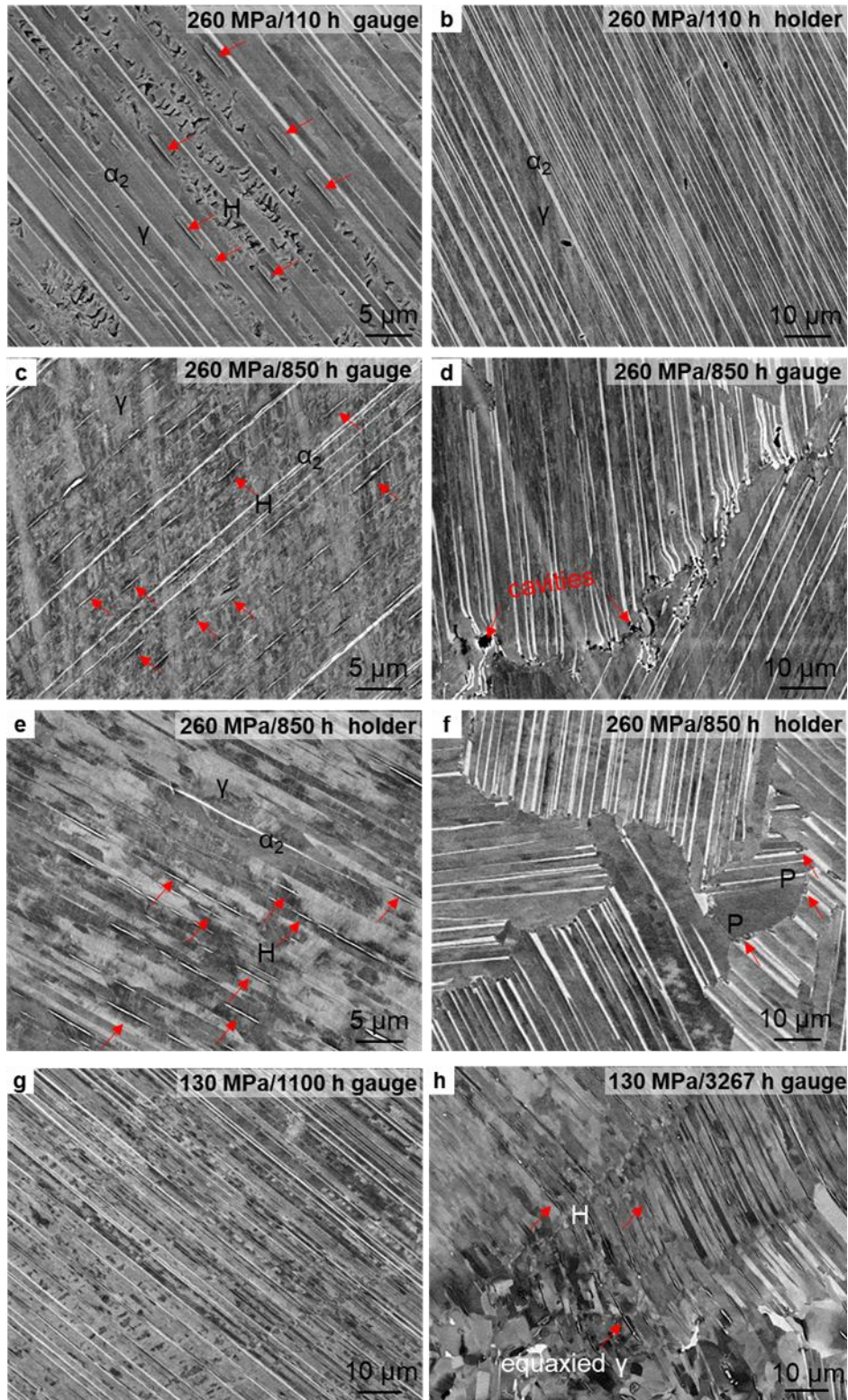


Fig. 4 SEM investigations in back-scattered electron mode of the microstructure evolution during creep at 850 °C for different times. (a) 260 MPa/110 h, in the gauge section, (b) 260 MPa/110 h, in the holder section, (c, d) 260 MPa/850 h, in the gauge section, and (e, f) 260 MPa/850 h, in the holder section, (g) 130 MPa/1100 h, in the gauge section, (h) 130 MPa/3267 h, in the gauge section

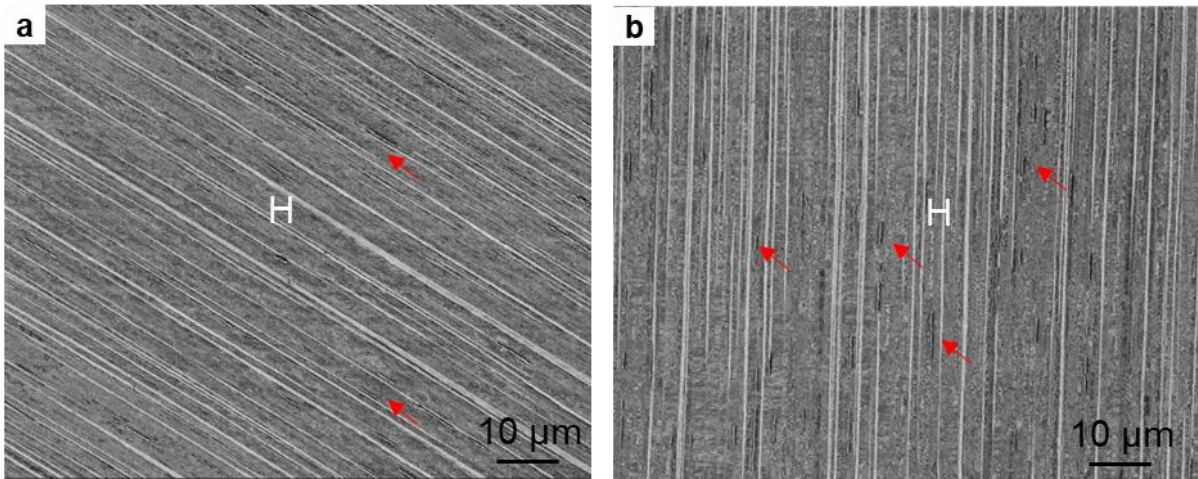


Fig. 5 SEM investigations in back-scattered electron mode of the microstructure evolution during creep at 750 °C for 1200 h in the gauge section under stress of (a) 130 and (b) 260 MPa

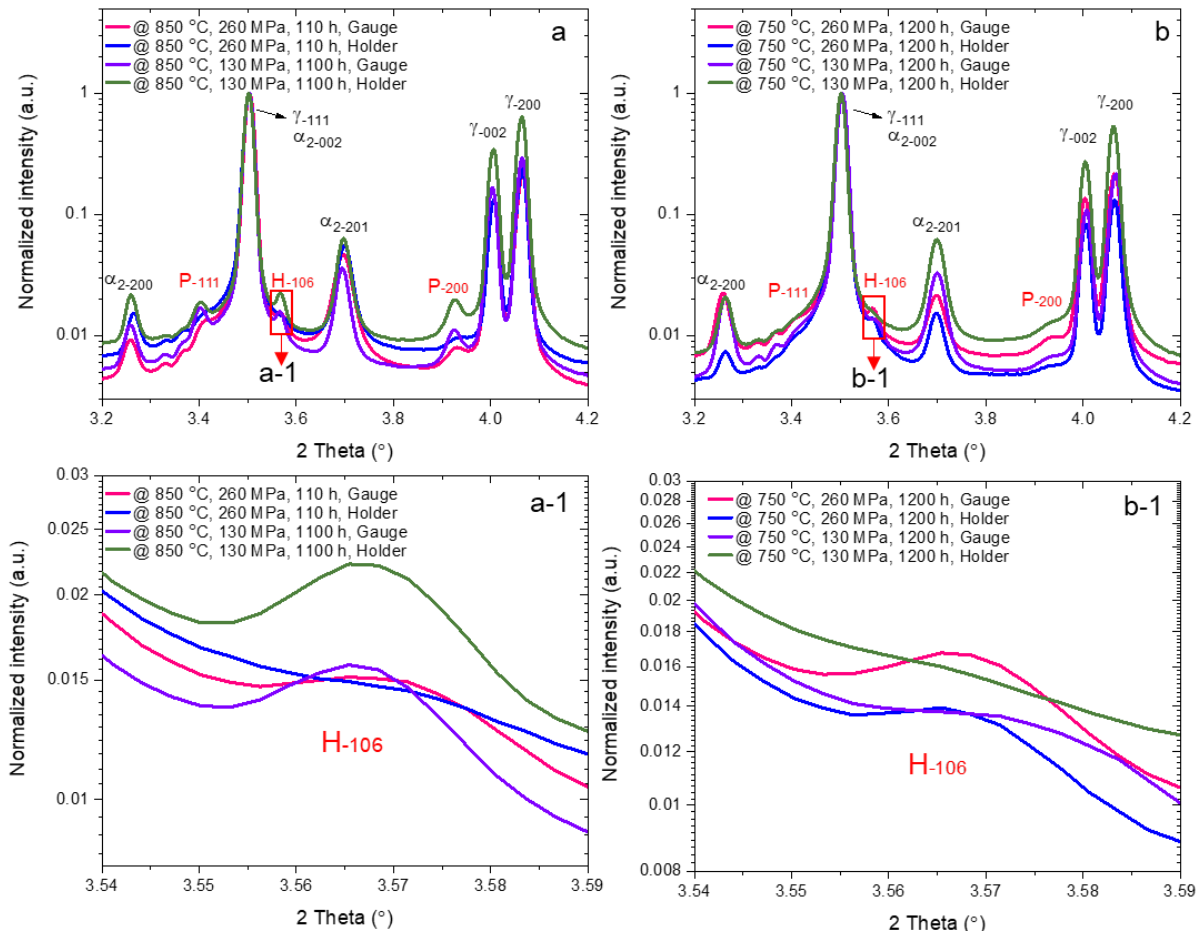


Fig. 6 HEXRD spectra of specimens after creep. (a) Crept at 850 °C, (a-1) enlarged spectra for the marked region in (a), (b) crept at 750 °C, and (b-1) enlarged spectra for the marked region in (b)

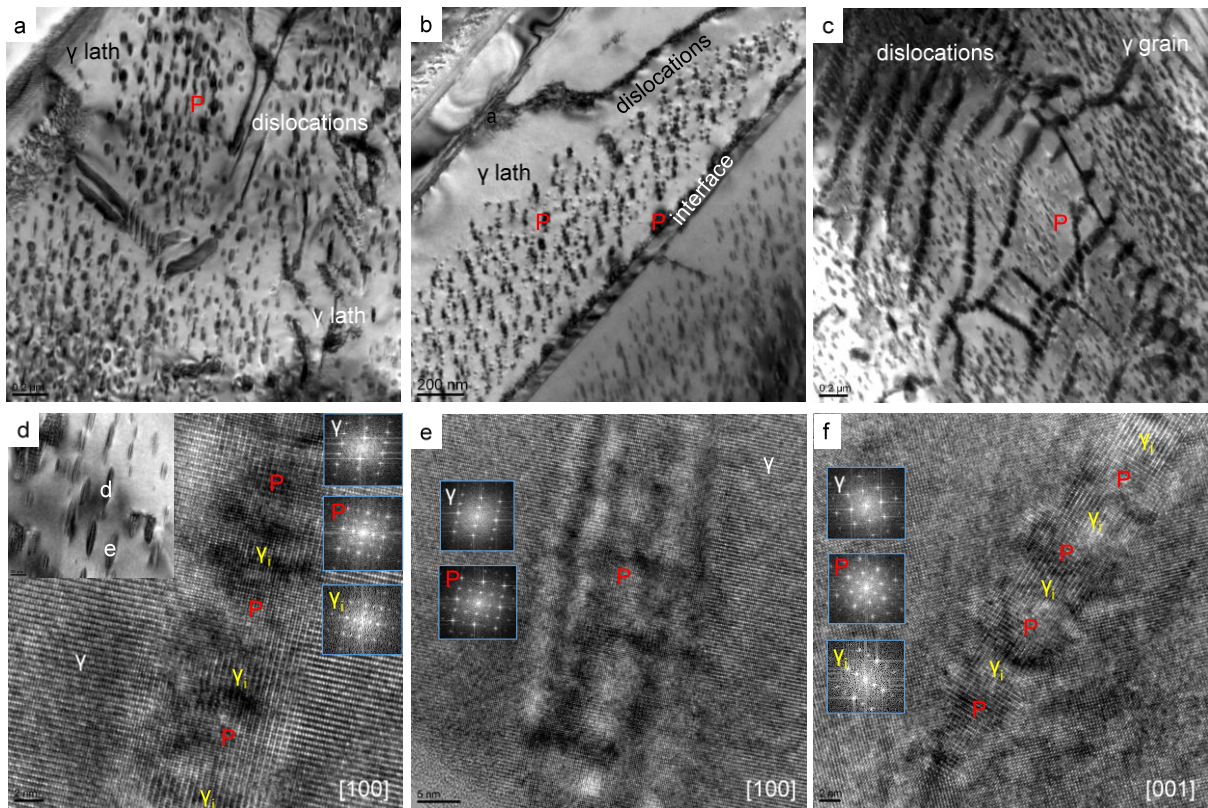


Fig. 7 TEM and HRTEM investigation of the P-carbides in specimens crept at 750 °C for 1200 h. P-carbides form (a) in the γ laths, (b) along the lamellar interfaces and (c) in the γ grains. P-carbides split in the γ phase (d, e, and f). (d) The needle-like projection of a carbide conglomerate viewed along the $[100]_{\gamma}$ orientation, the inserted image is a low magnification of d and e, (e) the plate-like projection of a carbide conglomerate recorded along the $[100]_{\gamma}$ orientation, and (f) the cross-section of a carbide conglomerate along the $[001]_{\gamma}$ orientation

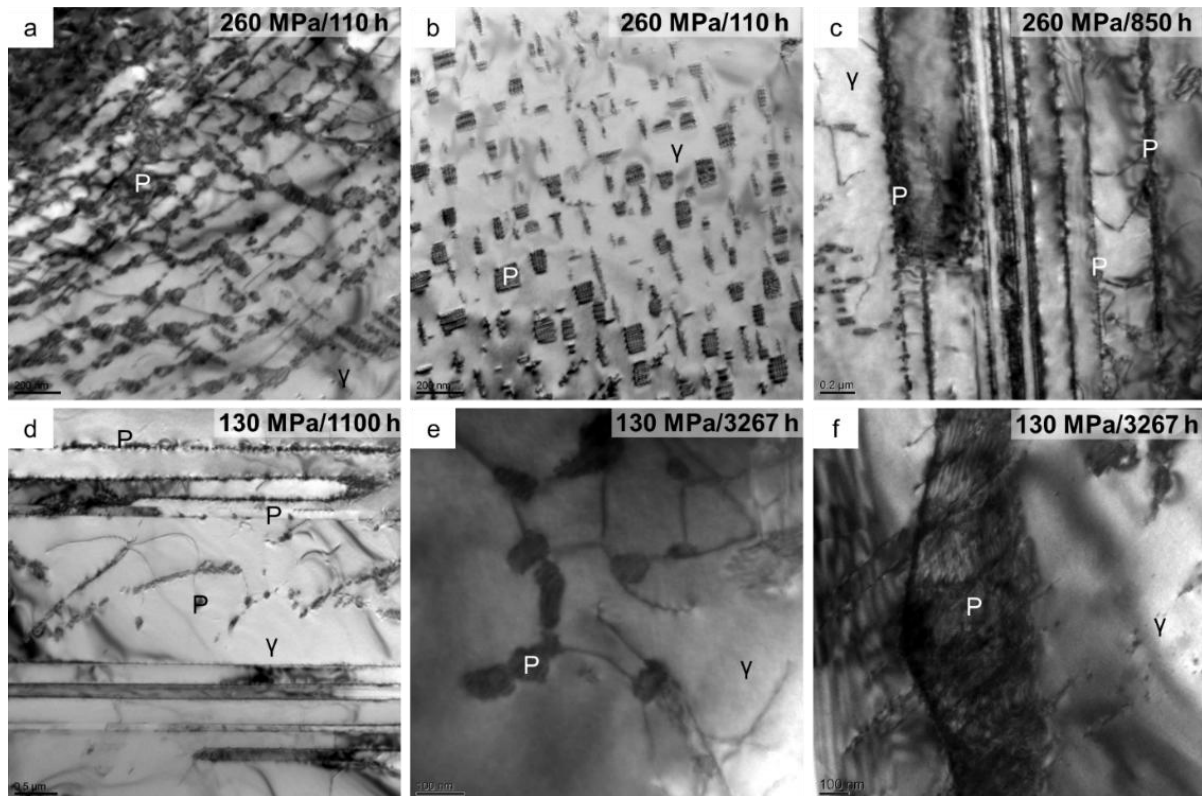


Fig. 8 TEM of the P-carbides in the specimens crept at 850 °C for different times: under 260 MPa for 110 h (a) P-carbides interact with dislocations, (b) P-carbides split in the γ phase; under 260 MPa for 850 h (c) P-carbides at dislocations and lamellar interfaces; under 130 MPa for 1100 h (d) P-carbides at dislocations and lamellar interfaces; under 130 MPa for 3267 h (e) only a few P-carbides remain at dislocations and lamellar interfaces, and (f) coarse P-carbides exist at grain boundaries

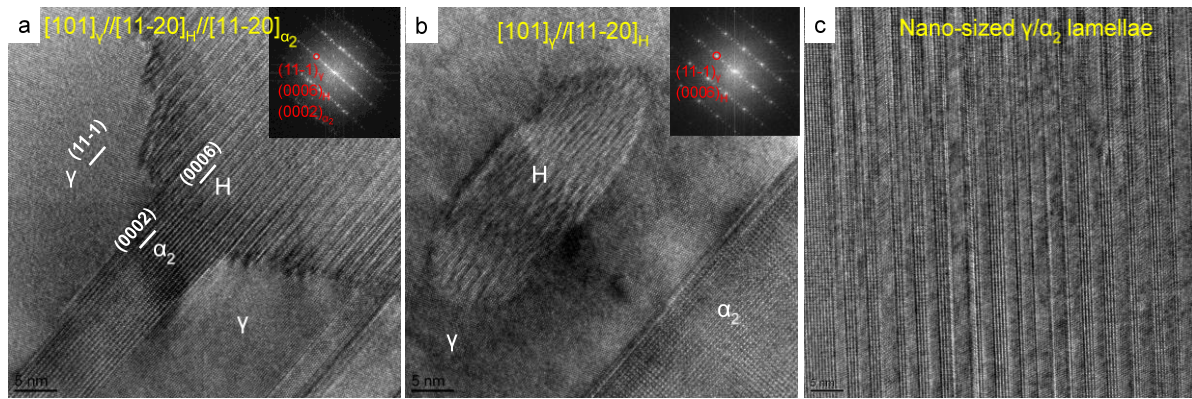


Fig. 9 HRTEM investigation of the H-carbides. (a) H-carbides form along the γ/α_2 interfaces (b) H-carbides precipitate in the γ lath, and (c) α_2 laths have decomposed into nano-sized γ/α_2 lamellae